Biophysical Reports

ARTICLE

Tracking protein transitions through fluorescence spectral phasor analysis with ACDAN

Leandro Cruz Rodríguez,[1] Nahuel Naum Foressi,[1] and María Soledad Celej[1,*]

[1]Departamento de Química Biológica Ranwel Caputto, Centro de Investigaciones en Química Biológica de Córdoba (CIQUIBIC, CONICET), Facultad de Ciencias Químicas, Universidad Nacional de Córdoba, Haya de la Torre y Medina Allende, Ciudad Universitaria, Córdoba, Argentina

ABSTRACT This study investigates the use of spectral phasor analysis, hyperspectral imaging, and 6-acetyl-2-dimethylaminonaphthalene (ACDAN) fluorescence to explore key protein transitions: unfolding, amyloid aggregation, and liquid-liquid phase separation. We show that ACDAN fluorescence can sensitively detect subtle conformational changes before the complete protein unfolds, revealing early microenvironmental shifts. During amyloid formation, ACDAN identifies solvent dipolar relaxation events undetectable by conventional thioflavin T, providing critical insight into early aggregation events. Additionally, we map the physicochemical properties of protein biocondensates and highlight distinct microenvironments within these condensates, emphasizing the significance of dipolar relaxation in phase-separated systems. The approach provides a flexible and user-friendly toolkit for studying protein transitions, which can be easily implemented in commercial spectrofluorometers and microscopes.

WHY IT MATTERS Understanding protein conformational transitions is fundamental to unraveling key biological processes and diseases. This study presents a simple yet powerful approach employing spectral phasor analysis, hyperspectral imaging, and 6-acetyl-2-dimethylaminonaphthalene fluorescence to investigate protein behavior. By capturing subtle shifts before unfolding, identifying the initial stages of amyloid aggregation, and mapping the microenvironments of protein biocondensates, the method offers deeper insights into protein stability and phase transitions. The approach is accessible and easily implemented, making it a valuable tool for various biochemical and biomedical applications, advancing research in protein dynamics, disease pathology, and therapeutic development.

INTRODUCTION

Proteins are essential macromolecules in biology. They play a crucial role in nearly all cellular processes, from catalyzing biochemical reactions to structural support for cells and tissues, and as signaling molecules regulating communication within and between cells. Protein (un)structure, dynamics, and stability are essential to preserve their activity and function. Understanding proteins is fundamental to understanding life processes, diseases, and biotechnological advancements.

Following Anfinsen's discovery that proteins can be reversibly folded outside of a cell (1), researchers are exploring the in vitro folding/unfolding process to understand the mechanisms and the thermodynamics by which polypeptides reach their lowest free energy states. The fundamental principles of protein folding have practical applications in the understanding of several pathologies, in the design of novel proteins with specific functions, and in the formulation of protein pharmaceuticals (2). Although the traditional view of a functional protein sees it as a highly constrained conformational ensemble, many such proteins may contain significantly disordered regions or may be largely unstructured, and these are often referred to as intrinsically disordered proteins (IDPs). Despite the complex proteostasis network

Submitted February 22, 2025, and accepted for publication April 14, 2025.

*Correspondence: mcelej@unc.edu.ar

Nahuel Naum Foressi's present address is Neurobiology & Biophysics, University of Washington School of Medicine, Seattle, Washington

Leandro Cruz Rodríguez and Nahuel Naum Foressi contributed equally to this work.

Editor: Jorg Enderlein.

https://doi.org/10.1016/j.bpr.2025.100209

that functions to maintain proteins in their soluble state, they can convert into nonfunctional and potentially harmful protein aggregates under certain circumstances. Both globular proteins and IDPs have been implicated in the formation of these aggregates, more frequently amyloids, which are associated with human diseases (3). Seven out of the 37 polypeptides associated with amyloid disease form deposits in the central nervous system, giving rise to neurodegenerative conditions, such as Alzheimer's and Parkinson's diseases. These disorders are among the most prevalent progressive age-related neuropathies and constitute a major cause of disability and mortality worldwide (4,5). There is an increasing interest in exploring the link between amyloid aggregation and liquid-liquid phase separation (LLPS), i.e., the thermodynamic process in which a homogeneous solution of macromolecules separates into two compositionally distinct liquid phases, with a dense polymer-rich phase coexisting with a diluted phase. Although recognized as a crucial mechanism governing the spatiotemporal organization of biochemical pathways (6), increasing evidence suggests that the formation of condensates through LLPS may be one pathway leading to protein aggregation (7,8). The hypothesis has sparked a revolution in research and therapeutic advancements for neurodegenerative disorders.

Several techniques can be employed to undergo biochemical and biophysical studies of proteins in vitro, in cells, and in vivo. Among these, fluorescence spectroscopy is widely used due to its technical simplicity, high versatility, and well-established theoretical framework of chemical and physical processes (9,10). It has been a cornerstone technique for investigating protein conformational changes. It offers advantages over other spectroscopic methods through its superb sensitivity, high-resolution capabilities, and the continuous development of novel fluorophores (11). Traditional methods, like monitoring intrinsic tryptophan (Trp) fluorescence, have offered valuable insights into protein folding/unfolding transitions. However, these methods often fall short in revealing information about changes in the local environment (microenvironment) that occur during complex protein transitions, such as amyloid formation and LLPS. Measuring microenvironmental properties is crucial, as they significantly influence the physical and chemical behaviors of surrounding molecules. Environment-sensitive dyes change their emission characteristics (intensity and/or color) in response to the properties of their solvation shell. As such, they are universal tools in fluorescence sensing and imaging, responding to any biomolecular interaction or change in biomolecular organization that modifies their local microenvironment (12). A major contribution in this field came from the pioneering work of Gregorio Weber, who introduced a series of fluorescent probes known as naphthalene derivatives, commonly referred to as the DAN family (13). Among these, 6-acetyl-2-dimethylaminonaphthalene (ACDAN), a water-soluble member of the DAN family, has gained considerable attention for its ability to sense solvent relaxation phenomena in biomimetic systems, cells, and tissues (14). On the other hand, the phasor analysis (15,16), either lifetime or spectral, has improved the ease and intuitiveness of the data analysis of cuvette and imaging fluorescence measurements (17–19). Spectral phasor (SP) analysis is a model-free methodology that converts emission spectra into a two-dimensional plot, effectively capturing variation in the center of mass of the spectrum (phase) and the spectrum's full width at half maximum (modulation) (17). These features are intimately related to alterations in the local microenvironment of the fluorophore. Here, we combine SP analysis and ACDAN fluorescence to explore three key protein transitions: unfolding, amyloid aggregation, and LLPS. Our findings demonstrate that this approach provides valuable insights that enhance the information obtained from traditional methods.

MATERIALS AND METHODS

Reagents

Polyethylene glycol 6000 (PEG-6000), spermine (Spe), human serum albumin (HSA), guanidinium hydrochloride (GuHCl), and thioflavin T (ThioT) were purchased from Sigma-Aldrich (St. Louis, Missouri). ACDAN was a kind gift from Professors Luis A. Bagatolli and Leonel Malacrida. Buffer solutions were of analytical grade. Milli-Q water was obtained from an ion exchange resin. Solutions were filtered through a 0.22-μm-size membrane.

Protein expression and purification

Recombinant human α-synuclein (α-syn) was expressed in *Escherichia coli* BL21(DE3) cells transformed with a pT7-7 plasmid encoding for the protein as described previously (20). For specific labeling with thiol-reactive fluorophores, the residue Ala^{140} was replaced by Cys (α-syn-A140C). The variant α-syn-A140C was expressed and purified as the wild-type protein, adding 5 mM DTT (Genbiotech, San Francisco, California) in the elution buffer to avoid disulfide bridge formation (20). The sequence encoding for human full-length Tau (2N4R) was cloned into a pET-16b expression vector (GeneUniversal, Newark, Delaware) and was preceded by a tobacco etch virus protease-recognition sequence fused at the N-terminus to a poly-histidine tag. The protein was expressed in Rosetta 2 cells and purified as described in (21).

HSA chemical denaturation assay

30 mg mL^{-1} HSA and 9 M GuHCl stock solutions were prepared in 25 mM Tris-HCl buffer (pH 7.4). 150 μM ACDAN was prepared in the

same buffer and stored in amber-colored Eppendorf tubes at 4°C for no longer than 3 weeks. Protein concentration was quantified by absorbance using an $\epsilon^{280\ nm}$ of 35,700 M^{-1} cm^{-1}. Solutions of 50 μM HSA at increasing concentrations of GuHCl were equilibrated for 5 min before measurements. ACDAN was added to a final concentration of 1 μM. Unfolding curves were monitored by Trp and ACDAN fluorescence. Experiments were performed in triplicate (Trp) or duplicate (ACDAN) and analyzed independently.

The midpoint of denaturation ($[GuHCl]_{1/2}$) was obtained by fitting the data (λ_{max} or the fraction of unfolded protein calculated from the phasors) with the Boltzmann sigmoidal relation:

$$y = A_2 + \frac{A_1 - A_2}{1 + e^{\frac{[GuHCl] - [GuHCl]_{1/2}}{dx}}}, \quad (1)$$

where A_1 and A_2 are the asymptotes (0 and 1, respectively, for the phasor analysis) and dx is related to the slope at $[GuHCl]_{1/2}$.

Fibrillation assay

The aggregation of 100 μM α-syn in the presence of 100 μM Spe was carried out in 25 mM Tris-HCl (pH 7.4), 0.01% NaN_3, containing 10% PEG-6000 as a crowding agent. Samples were incubated for up to 48 h at 37°C under quiescent conditions in a Dalvo incubator. Aliquots were withdrawn at different points and mixed with 5 μM ThioT in glycine buffer (pH 8.2) to a final protein concentration of 0.25 μM. Simultaneously, aliquots mixed with 5 μM ACDAN in 25 mM Tris-HCl buffer (pH 7.4) were measured. Experiments were performed in duplicate and analyzed independently.

Kinetic traces of amyloid formation monitored by ThioT were analyzed assuming a nucleation polymerization model according to an equation for the fractional normalized amyloid conversion ($\gamma(t)$):

$$\gamma(t) = \frac{1 - e^{-k_{app}t}}{1 + e^{-k_{app}\left(t - t_{1/2}\right)}}, \quad (2)$$

where k_{app} is the apparent rate constant for the incorporation of monomers at the growth point located in aggregates and $t_{1/2}$ is the time point of 50% of apparent conversion. In this model, $\gamma(t)$ is the fractional ThioT signal without independent determination of monomer conversion (22). Fibril formation at the endpoint of aggregation was confirmed by atomic force microscopy.

LLPS assay

Mixed α-syn/Tau and α-syn-Spe induced liquid droplets were obtained according to (21). Briefly, 100 μM α-syn in 25 mM Tris-HCl (pH 7.4), 10% PEG-6000, 0.01% Na-azide, was mixed with 1 μM Tau or 100 μM Spe at room temperature. Tau liquid droplets were formed by incubating 5 μM protein solution in the same buffer. Droplet formation was monitored by fluorescence microscopy within the first hour of incubation, as described below. Experiments were performed in triplicate.

Fluorescence spectroscopy

Corrected steady-state emission spectra were acquired at room temperature in a Cary Eclipse spectrofluorometer (Agilent Technologies, Lexington, Massachusetts). Trp and ACDAN fluorescence were measured using a 3 mm optical path length cell and excited at 295 and 370 nm, respectively, with spectral bandwidths set at 10 and 5 nm, respectively. ThioT measurements were performed using λ_{exc} = 446 nm, spectral bandwidths of 10 nm, and a 1 cm path cuvette.

Fluorescence microscopy

Liquid droplets were visualized using an Olympus FV1000 microscope with a PlanApo *N* 60×/1.42 numerical aperture oil immersion objective under differential interference contrast and fluorescence modes. Aliquots from each LLPS assay were incubated with 10 μM of ACDAN and placed in Nunc Lab-Tek II chambers (Thermo Fisher Scientific, Waltham, Massachusetts) with a microscopic quality glass of 0.17 mm thickness whose surface was passivated with a 1% w/v bovine serum albumin solution to avoid nonspecific interactions between the sample and the glass. The confocal spectral imaging experiments were performed by exciting at 405 nm and collecting the emission light between 430 and 600 nm with a resolution of 1 nm. The emission spectra collected from specific regions of interest were normalized to enable easier comparison.

Atomic force microscopy

Aliquots (10 μL) of the samples were diluted with water and spin coated on freshly cleaved mica surfaces. The spin-coated cycles were 3000 rpm for 1 min and 500 rpm for 1 min. Images of 512 × 512 pixels were collected at a scanning rate between 0.3 and 0.4 in s^{-1} on a multimode atomic force microscope (SPM, Agilent Technology 5500). All experiments were carried out at room temperature. The images were processed using Gwyddion software.

HSI

Hyperspectral imaging (HSI) data were collected by registering ACDAN emission spectra at 10 nm intervals, from 420 to 720 nm (a total of 30 spectra). Spatial information was obtained using 256 × 256 pixel fields with a pixel size of ∼100 nm. The acquisition duration was 90 s using the 405 nm excitation line of a diode laser, a BS20/80 beam splitter, and a dwell time of 10 μs/pixel. The spectral configuration of a Hamamatzu AW 064600 detector built into an Olympus FV 1000 microscope was used for all measurements.

SP approach

The SP approach is a fast and robust method to approach complex processes without the necessity for preconceived models that can be applied to spectral data obtained from commercial fluorometers and microscopes. The method transforms the emission spectrum into a phasor, which contains all the information reported by the probe and represented by the coordinates $G_{(\lambda)}$ and $S_{(\lambda)}$ calculated as follows:

$$G_{(\lambda)} = \frac{\sum_\lambda F(\lambda) cos\left(\frac{2\pi n(\lambda - \lambda_0)}{L}\right)}{\sum_\lambda F(\lambda)} \text{ and} \quad (3)$$

$$S_{(\lambda)} = \frac{\sum_\lambda F(\lambda) sin\left(\frac{2\pi n(\lambda - \lambda_0)}{L}\right)}{\sum_\lambda F(\lambda)}, \quad (4)$$

where $F(\lambda)$ are the fluorescence intensity values, λ_0 is the initial wavelength of the spectrum, L is the total range of wavelength used for the spectrum ($\lambda_{max} - \lambda_0$), and n is the harmonic value ($n = 1$ in our case) (23,24). The angular position of the phasor is related to the center of mass of the spectrum, with red-shifted spectra displaced counterclockwise in the phasor plot (Fig. 1 *A*). The radial position, an indicator of the heterogeneity of the probe's environment, is inversely related to the full width at half maximum and moves toward the center of the plot as the width increases (Fig. 1 *B*). Phasors allow easy identification of single or combined spectra and the quantification of the fraction of multiple components using the linear combination rule (Fig. 1 *C*). In the phasor analysis of fluorescence images (Fig. 1 *D*), each pixel in the image has an associated point in the phasor plot, and each point in the phasor plot maps to pixels and features in the image (24). $G_{(\lambda)}$ and $S_{(\lambda)}$ values of each pixel within an image provide information about the heterogeneity of the environment where the probe is located (25).

Cuvette SP analysis and visualization were performed using the open-source Java software found at https://github.com/lsocas314/Spectrasor/releases/tag/v1.0 (26), and HSI processing and visualization were conducted using simFCS software (https://www.lfd.uci.edu/globals/). For the analysis of condensates under different experimental conditions, the phasors for the diluted phase were excluded.

The distinct environments were characterized by measuring the extent of dipolar relaxation (DR). DR refers to the process by which the orientation of solvent dipoles around a fluorescent probe relaxes after excitation. Changes in DR indicate alterations in the local polarity, viscosity, and environment dynamics surrounding the probe (9,27). In protein condensates, variations in DR detected by ACDAN fluorescence can reveal differences in the microenvironmental properties within the condensates, such as hydrophobicity or molecular ordering.

The data were analyzed using a two-cursor approach based on the method described by Mangiarotti et al. (25). This method was selected because the phasor cloud from the different condensates can be represented as two states of low and high DR, allowing us to apply the linear properties of phasor space. The histograms display the number of pixels for each step along the line between the two cursors, normalized by the total pixel count. The center of mass for each distribution, a measure of the extent of DR within each droplet, was calculated as

$$CM = \sum_{i=0}^{i=1} F_i i \Big/ \sum_{i=0}^{i=1} F_i, \tag{5}$$

where F_i represents the fraction for DR. Regardless of the specific positions chosen for the cursors on the phasor plot, any difference in the center of mass of the histograms is determined through statistical analysis. Calculated DR values are presented in box-and-whisker plots for clarity. Statistical significance was determined using one-way ANOVA. Asterisks indicate statistical significance (**$p < 0.01$).

RESULTS AND DISCUSSION

ACDAN paired with SP analysis reveals conformation changes before protein unfolding

Trp fluorescence is a common readout used to study protein denaturation due to the bathochromic shift observed upon exposure to a polar environment. Previous studies have demonstrated the usefulness of the SP method for investigating protein denaturation (26,28,29) and homo-oligomerization (30). Here, we

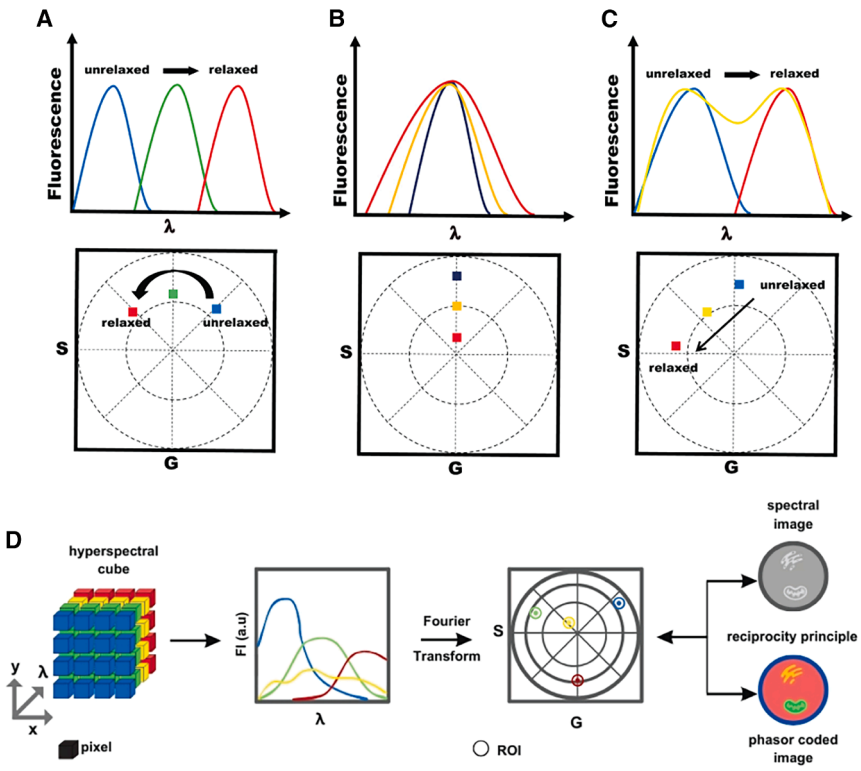

FIGURE 1 Illustration of SP analysis. (*A–C*) Schematics of fluorescence spectra (*top*) and the corresponding SP plots (*bottom*). Bathochromic shifts move the position of the phasor in a counterclockwise direction (*A*). Increasing the spectral width moves the phasor toward the center of the plot (*B*). The linear combination property enables the quantification of the fractions of multiple components (*C*). (*D*) Schematics of phasor plots of HSI. The data structure in HSI is *xy* (space) and λ. SP transformation for single components and mixtures can be represented in the SP plot. The reciprocity principle enables the selection of regions of interest on the phasor plot (*color circles*) and generates a phasor-coded image for all pixels in an image.

evaluate the effectiveness of this method by analyzing the emissions of Trp and ACDAN to monitor chemically induced HSA denaturation in a complementary manner. HSA is a vital blood plasma protein that transports various endogenous and exogenous molecules, including drugs, fatty acids, and hormones (31), which is frequently used as a model for folding studies.

HSA contains a single Trp residue (Trp^{214}) located in a hydrophobic cavity within subdomain IIA, which corresponds to the Sudlow I ligand-binding site (31,32). Fig. 2 *A* shows the normalized Trp fluorescence spectra at increasing concentrations of GuHCl. Under native conditions, Trp emission is centered at 348 nm and shifts to 360 nm upon denaturation. These changes indicate that Trp becomes more solvent accessible, suggesting the unfolding of domain II. Although the peak position is not, a priori, proportional to the population of the states and could lead to a biased assignment toward the state with the higher quantum yield (33), such as the native state in our case, the shift in λ_{max} is frequently used to monitor the equilibrium unfolding transition, as shown in Fig. 2 *C*. From these data, we estimated the midpoint of denaturation $[GuHCl]_{1/2}$ to be ~3.33 M, a free energy of unfolding $\Delta G^{o}_{(H_2O)}$ of ~2 kcal mol^{-1}, and an *m* value of ~0.6 kcal mol^{-1} M^{-1}, which correlate with previous reports (34). Then, we constructed the SP plot from the Trp emission spectra (Fig. 2 *B*). The displacement of the phasor in the phasor space can be reasonably approximated by a linear trajectory, reflecting the conformational transition from which the fractional contribution of the denatured state can be calculated (Fig. 2 *C*). The denaturation profile obtained from this method matched the profile derived from the shift in λ_{max}, and similar equilibrium unfolding parameters were calculated.

ACDAN binds to bovine serum albumin in presumable hydrophobic pockets that could also include charged or polar amino acids (35). Thus, it is reasonable to expect that ACDAN also binds to HSA. Fig. 2 *D* shows normalized emission spectra of ACDAN in the presence of HSA at increasing amounts of GuHCl. In the absence of a denaturant, ACDAN showed a peak at 460 nm, indicating a constrained environment. As the amount of GuHCl increased, a shoulder at ~520 nm (relaxed) emerged, becoming dominant at higher GuHCl concentrations. These spectral changes are likely due to the release of the bound dye resulting from the loss of the HSA tertiary structure. Interestingly, the SP plot (Fig. 2, *E* and *F*) displays a clockwise rotation of the phasor at GuHCl concentrations lower than the midpoint of denaturation. This suggests a more restricted environment around the probe before protein unfolding. Structural studies using small-angle X-ray scattering have demonstrated that HSA

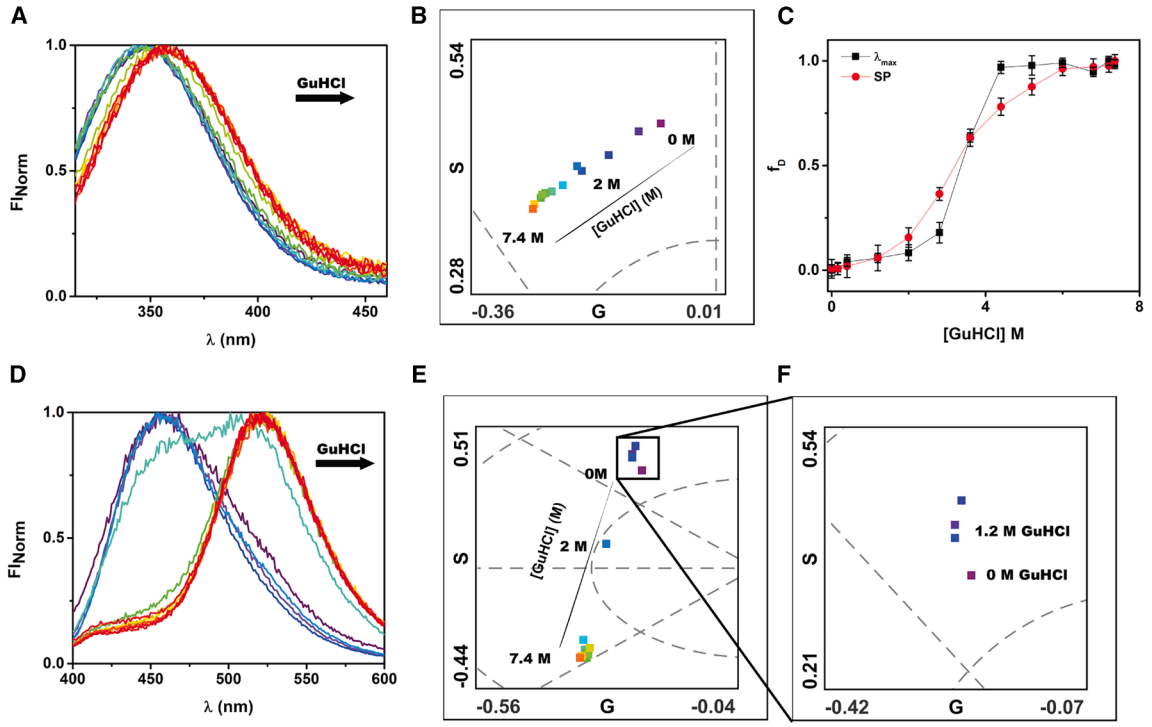

FIGURE 2 SP of ACDAN emission reveals a conformational change at low GuHCl concentrations. Representative normalized Trp (*A*) and ACDAN (*D*) fluorescence spectra along the corresponding SP plots (*B* and *E*) of GuHCl-induced HSA chemical denaturation. (*C*) Denaturation profiles obtained from Trp spectral shifts (■) and SP plot (●). (*F*) Magnified section of ACDAN SP plot at low GuHCl concentrations.

can adopt more compact conformations at low concentrations of denaturing agents (34,36). Additionally, a thermodynamic analysis of calorimetric traces for bovine serum albumin in the presence of GuHCl indicated a stabilizing effect on the native state at low denaturant concentrations (37).

These data highlight the significance of the SP approach as a valuable tool in protein spectroscopy. Furthermore, when combined with environment-sensitive dyes, it offers additional insights into the unfolding process of both soluble and membrane proteins (26,28–30).

ACDAN paired with SP analysis reveals early events during amyloid formation

Amyloid formation is another protein transition that has gained considerable attention due to its functional and pathological implications. Over the years, extensive efforts have been made to design new sensors and techniques to unravel protein association dynamics. To this end, we assessed the effectiveness of ACDAN and the SP approach for monitoring protein fibrillation, comparing them with the widely used ThioT fluorescence method. We used α-syn aggregation in the presence of Spe as our model system. α-syn is an IDP that accumulates into insoluble amyloid fibrils pathognomonic of Parkinson's disease and related neurodegenerative disorders. Spe is a biogenic tetramine that is typically elevated in age-related neuropathies (38) and has been shown to accelerate α-syn aggregation (39).

Fig. 3 shows the fluorescence spectra of ThioT at different time points during Spe-induced α-syn fibrillation (Fig. 3 *A*), along with the normalized kinetic aggregation curve (Fig. 3 *C*). As expected, ThioT fluorescence, which senses the cross-β fibrillar structure, displayed a classical sigmoidal profile, typically attributed to a nucleation-polymerization mechanism. According to this model, nucleation centers form initially, and during the lag phase, they progress through oligomerization into an elongation phase, ultimately resulting in the formation of the characteristic fibrils (40). Analysis of the kinetic ThioT curve indicated that under our experimental conditions, α-syn forms fibrils with a lag time of $\sim$10 h, an aggregation $t_{1/2}$ of $\sim$15 h, and an apparent growth rate constant k_{app} of $\sim$0.38 h^{-1}. The presence of fibrils at the end of the aggregation was confirmed by atomic force microscopy (*inset*, Fig. 3 *C*).

The ACDAN emission spectra are included in Fig. 3 *B*. Initially, the emission maximum of ACDAN was located at 518 $\pm$ 5 nm, near the position observed in the buffer alone (525 $\pm$ 5 nm, data not shown). This slight blue shift may arise from nonspecific interactions between the naphthalene moiety and hydrophobic regions on the disordered monomeric proteins (41), as has been suggested

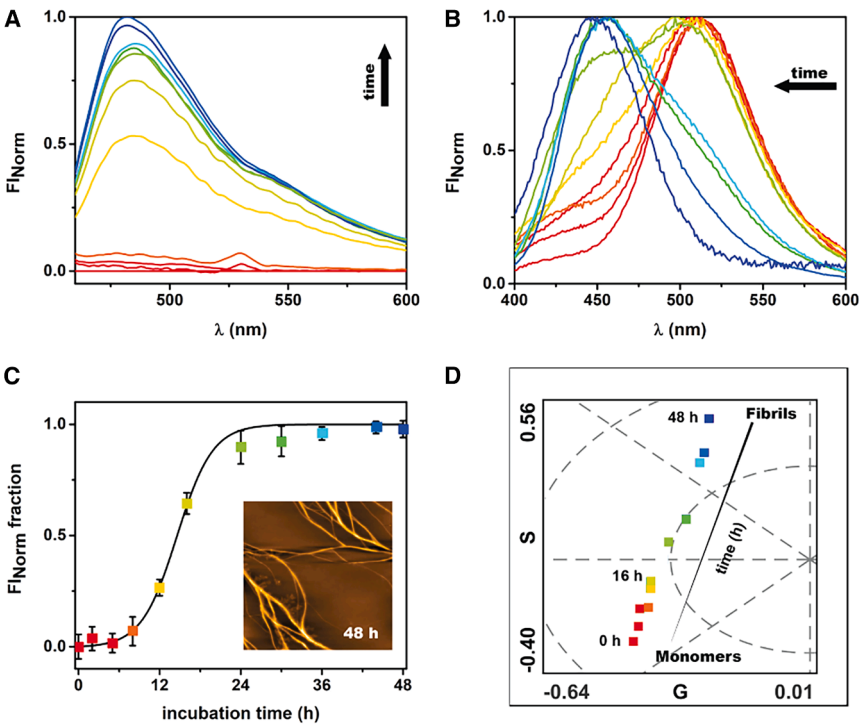

FIGURE 3 SP of ACDAN emission reveals early changes during amyloid formation. Normalized ThioT (*A*) and ACDAN (*B*) fluorescence spectra during quiescent fibrillation of α-syn in the presence of Spe. (*C*) Time course of α-syn aggregation sensed by ThioT. Inset: atomic force microscopy (AFM) image (5×5 μm) of the sample after 48 h of incubation. (*D*) SP plot of ACDAN during α-syn fibrillation.

for other naphthalene derivatives (22). As aggregation proceeded, a hypsochromic shift in the emission band and the appearance of a shoulder at about 455 nm were observed. The contribution of this blue-shifted band increased over time and was located at around 450 at the end of the aggregation. These changes can be easily visualized in the SP plot in Fig. 3 *D*. A continuous change from the initial monomeric state to the final fibrillar state can be visualized in the phasor space. The position of the phasor at the beginning of the aggregation indicates a more relaxed environment, characterized by higher homogeneity in the probe's surroundings in the monomeric state. During aggregation, a clockwise rotation and a shift toward the center were observed, representing a continuous reduction in the DR of the environment and higher heterogeneity around the probe.

The spectral changes described above responding to α-syn aggregation may be associated with global changes in solvent properties of the system and/or probe interactions with different aggregated states. Importantly, ACDAN is sensitive to changes occurring in the early steps of aggregation, which are not identified by the traditional ThioT probe. Water modulates the free energy landscape that dictates proteins' folding, structure, stability, flexibility, and functionality (42,43). Hydration water also plays a role in modulating atomic motions in IDPs, which typically exhibit a significantly greater exposed surface area when compared to a similarly sized globular protein. The increased mobility of hydration water and H-bonding in IDPs enables functional plasticity through enhanced protein flexibility (44). Therefore, changes in water dynamics can lead to lower desolvation energy barriers and decreased protein mobility, potentially increasing the likelihood of protein-protein interactions and aggregation (44,45). Indeed, changes in surface hydration water dynamics and solvent accessibility detected by Overhauser dynamic nuclear polarization of water interacting with stable nitroxide spin labels tethered to specific protein sites have been used to monitor protein aggregation (46,47). On the other hand, a myriad of conformational structures of α-syn exist at various stages of aggregation, including spheroids, chains of spheres, rings resembling circular protofibrils, acunas, and fully formed polymorphic fibrillar structures (48–50). Thus, the application of ACDAN and SP analysis represents a useful, accessible, and simple tool to investigate amyloid kinetics, which, in combination with other traditional techniques, has the potential to provide valuable information on the mechanism of amyloid formation.

ACDAN paired with SP analysis and HSI reveals distinct environments within protein biocondensates

α-syn and Tau, an IDP linked to Alzheimer's disease, undergo LLPS under various conditions in vitro, in cells, and in model organisms (51–55). Additionally, both proteins can coexist within liquid droplets (21,56–58), which has been associated with a possible mechanism underlying the pathological overlap between dementias and parkinsonism (55). In addition to the effect of Spe on α-syn aggregation mentioned above, Spe has also been linked to the phase separation of the protein (21) and the liquid-to-solid transition of α-syn/Tau condensates (58). At this point, we used ACDAN fluorescence and HSI to analyze the physicochemical environment in biologically relevant condensates at the nanometer scale: homotypic Tau droplets, heterotypic α-syn/Tau condensates, and α-syn droplets induced by Spe.

Fig. 4 *A* presents the differential interference contrast and fluorescence images of ACDAN for three different protein-containing condensates. The spectral resolution of ACDAN emission showed clear differences between the diluted and condensed phases (Fig. 4, *C–E*). The emission maximum of ACDAN in the diluted phase was $\sim$520 $\pm$ 5 nm for all three cases. In contrast, Tau droplets showed an emission maximum at 486 $\pm$ 3 nm, the α-syn/Tau condensates exhibited a slightly blue-shifted spectrum at 481 $\pm$ 2 nm, and the Spe-induced α-syn droplets displayed two distinct maxima, one at 522 $\pm$ 4 nm and the other at 479 $\pm$ 3 nm. These shifts to shorter wavelengths indicate that the condensates have a reduced DR environment as compared to the dilute phase, which is influenced by their compositions. Additionally, the red-shifted band in Spe-induced α-syn droplets localized with the position of the emission spectrum of the dispersed phase, which suggests a well-defined inner heterogeneity, probably at the two-phase interface.

To analyze the spectral shifts described above, we followed a similar approach described by Mangiarotti et al. (25), who applied a two-cursor analysis to extract the histograms for the pixel distribution along a linear phasor trajectory as a convenient way of visualizing the DR changes of ACDAN. Fig. 4 *F* depicts the phasor plot of the spectral emission of ACDAN within the three condensates, where the linear trajectory connects the low and high DR environments denoted by the green and red circles, respectively. The normalized histograms shown in Fig. 4 *G* indicate that DR values (x axis) decreased in the order Tau > Tau/α-syn > Spe-induced α-syn condensates. For a quantitative and statistical analysis of DR changes, we

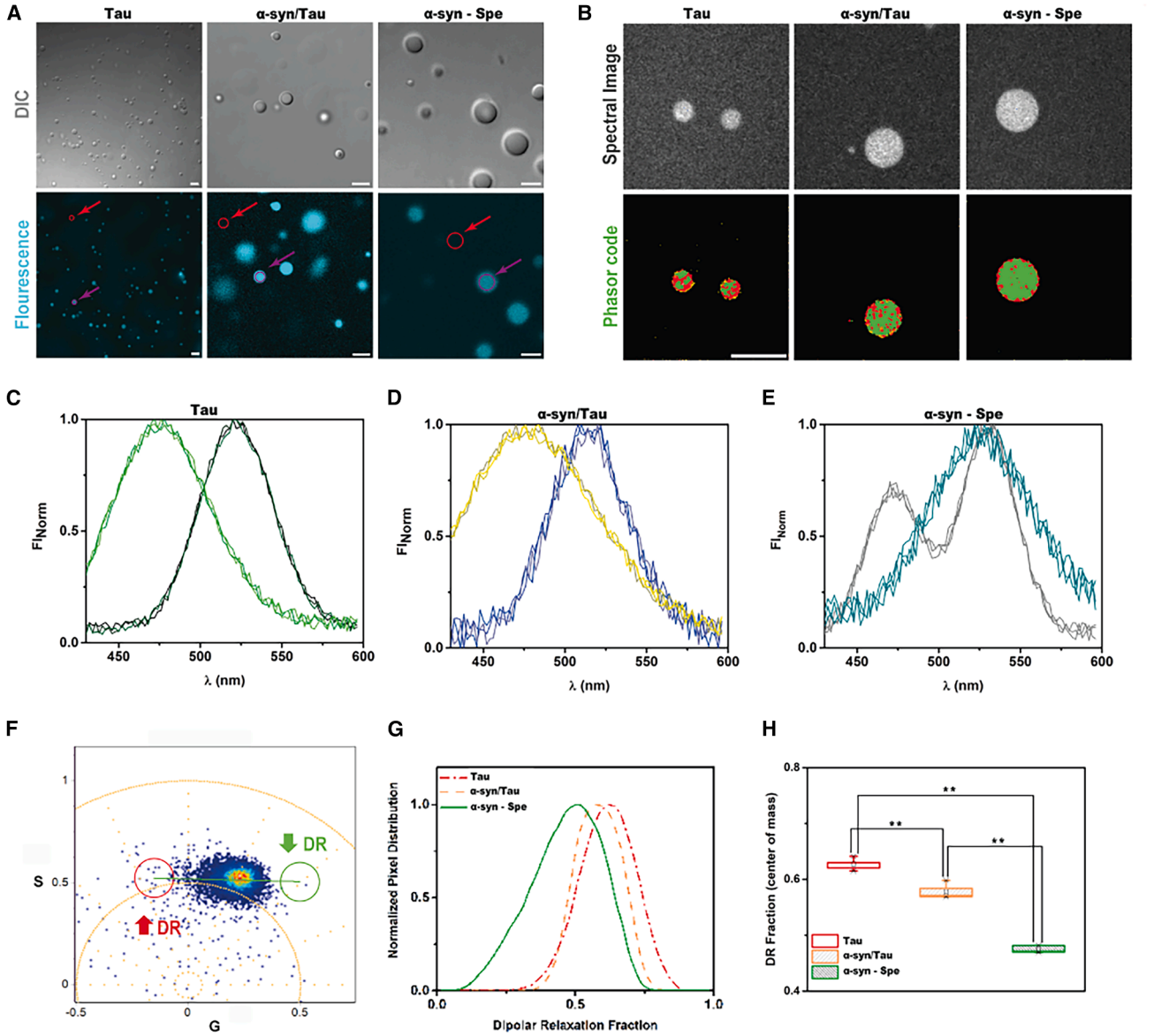

FIGURE 4 ACDAN reveals different environments inside protein condensates. (*A*) Differential interference contrast (DIC) and fluorescence microscopy images of homotypic Tau, heterotypic α-syn/Tau, and Spe-induced α-syn liquid droplets. Scale bars: 10 μm (Tau) and 5 μm (α-syn-containing droplets). (*B*) ACDAN HSI for representative droplets (*top*) and the corresponding phasor code images visualized with a bi-color pattern defined in (*F*). Scale bar: 5 μm. (*C–E*) ACDAN emission spectra inside and outside condensates: (*C*) —diluted (*olive*) and condensed (*green*) phase in homotypic Tau droplets; (*D*) —diluted (*blue*) and condensed (*yellow*) phase in heterotypic α-syn/Tau droplets; and (*E*) —diluted (*dark cyan*) and condensed (*gray*) phase in Spe-induced α-syn droplets. (*F*) ACDAN SP plot where two distinctive states are defined: higher (O) and lower (O) DR environments. Data correspond to all conditions. (*G*) Histograms from a two-cursor analysis showing the normalized distribution of pixels along the green line of (*F*). (*H*) Center of mass of DR distributions. Statistical significance was determined using one-way ANOVA. Asterisks indicate statistical significance (**p < 0.01).

calculated the center of mass of these histograms (Fig. 4 *H*). The three condensates differed significantly, with α-syn droplets induced by Spe displaying the lowest DR value, reflecting the most restricted environment.

Then, we took advantage of the reciprocity principle (18) of the phasor approach to obtain phasor-code images displaying the spatial distributions of phasors within the condensates, which are included in Fig. 4 *B*. Both Tau-containing condensates exhibited internal inhomogeneities that were distributed throughout the droplets. In contrast, Spe-induced α-syn condensates showed the highest proportion of green pixels, constituting most of the droplet's volume, whereas red pixels were localized at the droplet's exterior shell in contact with the diluted phase.

SP and HSI analyses of ACDAN fluorescence provide insights into the physicochemical properties of condensates. Our findings demonstrate that condensates differ from the dispersed phase and show varying physicochemical environments based on their composition. The lower DR values observed within the interior of the condensates suggest that these regions have a constrained environment where the reorientation of solvent molecules is limited. In the context of the intracellular environment, these results provide evidence that the composition of condensates, influenced by cellular conditions, modulates their biophysical properties, with both functional and pathological implications.

Recent studies have employed both experimental and computational methods to rationalize the selective partitioning of small molecules into condensates (59,60). The use of diverse chemical compounds spread over a wide range of partition coefficients suggested that a hydrophobic environment emerges upon the formation of condensates, which influences the distribution of molecules (59). This aligns with our observation that the interior of the condensates displays lower DR, indicating reduced solvent dynamics. Conversely, condensates formed by different proteins exhibit distinct partitioning patterns within a narrow range of partition coefficients. This observation supports the idea that different condensates possess unique chemical solvation environments (59,60). In this connection, our results denote that ACDAN fluorescence can distinguish subtle differences in solvent DR among compositionally different condensates. This finding is reinforced by recent reports indicating that ACDAN can differentiate between condensates formed by dengue and Zika viruses (61) and among glycinin condensates under varying salinity conditions (25).

Water is essential in the formation of protein droplets through LLPS. In environments where water activity is particularly low, the conditions become highly conducive to aggregation, both kinetically and thermodynamically, highlighting the critical nature of water in these processes (45). Thus, our findings align with increasing evidence that condensates likely serve as nucleation sites for pathological aggregation, especially in neurodegenerative conditions (62,63). Our analysis has revealed the presence of solvent DR heterogeneity within the three model condensates. On the one hand, the α-syn condensates induced by Spe exhibited a distinct rim on their surface, indicating a more relaxed environment at the boundary between the two coexisting phases. On the other hand, spatial inhomogeneities in solvent properties were detected in Tau-containing droplets. Recent experiments have shown that condensate interfaces influence the kinetics of amyloid fibril formation (64–69), highlighting the importance of condensate interfaces on the liquid-to-solid transition. In other cases, however, the amyloid-like aggregation was promoted within the droplets (58,63,70,71). Further research connecting protein aggregation foci and ACDAN fluorescent features could yield important insights into the physicochemical factors contributing to the initiation of condensate-mediated amyloid formation.

CONCLUSIONS

In this study, we underscore the power of the SP approach combined with ACDAN fluorescence as a valuable complementary tool for studying protein conformational transitions. By leveraging this method, we not only confirmed the equilibrium unfolding parameters of HSA derived from traditional spectral shifts but also identified subtle conformational changes before unfolding.

Beyond unfolding studies, we demonstrated that ACDAN fluorescence and SP analysis effectively capture early-stage structural changes during amyloid formation. Unlike the conventional ThioT method, which primarily detects mature fibrillar states, our approach highlighted solvent environment shifts occurring in the initial aggregation phases. The sensitivity of ACDAN to DR changes allowed us to track the dynamic transitions of α-syn, revealing a progressive restriction in solvent mobility that could contribute to nucleation and fibril growth. These results suggest that our technique offers a more comprehensive perspective on protein aggregation mechanisms, potentially aiding in the development of therapeutic strategies targeting early amyloid formation events.

Furthermore, our study on protein biocondensates uncovered distinct solvent environments within droplets. The ability of ACDAN fluorescence and HSI to map heterogeneities at the nanoscale provides a new lens for understanding condensate composition and stability, enhancing the current toolkit used for measuring condensate properties both in vitro and in cells. The differential DR patterns observed among Tau, α-syn/Tau, and Spe-induced α-syn droplets suggest that condensates create unique microenvironments influencing molecular partitioning and aggregation propensity. Given the growing recognition of condensates as precursors for pathological amyloid formation, our findings highlight the potential of ACDAN and SP analysis in unraveling the physicochemical factors that govern phase transitions and neurodegenerative disease progression.

ACKNOWLEDGMENTS

L.C.R. and N.N.F. acknowledge their PhD fellowships from Consejo Nacional de Investigaciones Científicas y Técnica (CONICET) and Secretaría de Ciencia y Tecnología, Universidad Nacional de Córdoba (SECyT-UNC). M.S.C. is a research member of CONICET. We thank the microscopy facilities of CEMINCO, Centro de Micro y Nanoscopía de Córdoba, CONICET-UNC (https://ceminco.conicet.unc.edu.ar/). This work was supported in part by grants from ANPCyT (grant FONCyT PICT 2019-0228), Secretaría de Ciencia y Tecnología, and Universidad Nacional de Córdoba (grant SECyT-UNC PIDTA 2023). This research was supported by Argentina's science and technology agencies despite the current political challenges facing the field. The authors would like to express their gratitude to the late Dr. Luis A. Bagatolli for his inspiration and valuable recommendations during the early stages of this work. They also thank Dr. Leonel Malacrida for his helpful insights and discussions. Additionally, they appreciate the support and contributions from all the members of the biophysical area at the Dpto. Química Biológica Ranwel Caputto-CIQUIBIC.

AUTHOR CONTRIBUTIONS

L.C.R. and N.N.F. designed and performed the research, analyzed the data, and wrote the original draft. M.S.C. supervised the study and wrote the manuscript. All authors discussed the results and contributed to the final manuscript.

DECLARATION OF INTERESTS

The authors declare no competing interests.

DECLARATION OF GENERATIVE AI AND AI-ASSISTED TECHNOLOGIES IN THE WRITING PROCESS

During the preparation of this work, the authors used Grammarly and ChatGPT in order to improve language and readability. After using this tool/service, the authors reviewed and edited the content as needed and take full responsibility for the content of the publication.

REFERENCES

1. Anfinsen, C. B. 1973. Principles that govern the folding of protein chains. *Science.* 181:223–230. https://doi.org/10.1126/science.181.4096.223.
2. Ebrahimi, S. B., and D. Samanta. 2023. Engineering protein-based therapeutics through structural and chemical design. *Nat. Commun.* 14:2411. https://doi.org/10.1038/s41467-023-38039-x.
3. Chiti, F., and C. M. Dobson. 2017. Protein Misfolding, Amyloid Formation, and Human Disease: A Summary of Progress Over the Last Decade. *Annu. Rev. Biochem.* 86:27–68. https://doi.org/10.1146/annurev-biochem-061516-045115.
4. WHO. 2023. World Health Organization, in Dementia: Key facts. https://www.who.int/news-room/fact-sheets/detail/dementia.
5. IHME. 2024. Institute for Health Metrics and Evaluation, in *Parkinson's disease—Level 3 cause.* https://www.healthdata.org/research-analysis/diseases-injuries-risks/factsheets/2021-parkinsons-disease-level-3-disease.
6. Banani, S. F., H. O. Lee, …, M. K. Rosen. 2017. Biomolecular condensates: organizers of cellular biochemistry. *Nat. Rev. Mol. Cell Biol.* 18:285–298. https://doi.org/10.1038/nrm.2017.7.
7. Elbaum-Garfinkle, S. 2019. Matter over mind: Liquid phase separation and neurodegeneration. *J. Biol. Chem.* 294:7160–7168. https://doi.org/10.1074/jbc.REV118.001188.
8. Zbinden, A., M. Pérez-Berlanga, …, M. Polymenidou. 2020. Phase Separation and Neurodegenerative Diseases: A Disturbance in the Force. *Dev. Cell.* 55:45–68. https://doi.org/10.1016/j.devcel.2020.09.014.
9. Lakowicz, J. R. 2006. Principles of Fluorescence Spectroscopy, 3rd edition ed. Springer, Berlin.
10. Jameson, D. M. 2014. Introduction to Fluorescence. CRC Press.
11. Kyrychenko, A., and A. S. Ladokhin. 2024. Fluorescent Probes and Quenchers in Studies of Protein Folding and Protein-Lipid Interactions. *Chem. Rec.* 24:e202300232. https://doi.org/10.1002/tcr.202300232.
12. Klymchenko, A. S. 2017. Solvatochromic and Fluorogenic Dyes as Environment-Sensitive Probes: Design and Biological Applications. *Acc. Chem. Res.* 50:366–375. https://doi.org/10.1021/acs.accounts.6b00517.
13. Weber, G., and F. J. Farris. 1979. Synthesis and spectral properties of a hydrophobic fluorescent probe: 6-propionyl-2-(dimethylamino)naphthalene. *Biochemistry.* 18:3075–3078. https://doi.org/10.1021/bi00581a025.
14. Otaiza-Gonzalez, S., M. Cabadas, …, L. A. Bagatolli. 2022. The innards of the cell: studies of water dipolar relaxation using the ACDAN fluorescent probe. *Methods Appl. Fluoresc.* 10. https://doi.org/10.1088/2050-6120/ac8d4c.
15. Weber, G. 1981. Resolution of the fluorescence lifetimes in a heterogeneous system by phase and modulation measurements. *J. Phys. Chem.* 85:949–953. https://doi.org/10.1021/j150608a006.
16. Jameson, D. M., E. Gratton, and R. D. Hall. 1984. The Measurement and Analysis of Heterogeneous Emissions by Multifrequency Phase and Modulation Fluorometry. *Appl. Spectrosc. Rev.* 20:55–106. https://doi.org/10.1080/05704928408081716.
17. Malacrida, L., E. Gratton, and D. M. Jameson. 2015. Model-free methods to study membrane environmental probes: a comparison of the spectral phasor and generalized polarization approaches. *Methods Appl. Fluoresc.* 3:047001. https://doi.org/10.1088/2050-6120/3/4/047001.
18. Malacrida, L., S. Ranjit, …, E. Gratton. 2021. The Phasor Plot: A Universal Circle to Advance Fluorescence Lifetime Analysis and Interpretation. *Annu. Rev. Biophys.* 50:575–593. https://doi.org/10.1146/annurev-biophys-062920-063631.
19. Torrado, B., L. Malacrida, and S. Ranjit. 2022. Linear Combination Properties of the Phasor Space in Fluorescence Imaging. *Sensors.* 22:999.
20. Gallea, J. I., and M. S. Celej. 2014. Structural insights into amyloid oligomers of the Parkinson disease-related protein alpha-synuclein. *J. Biol. Chem.* 289:26733–26742. https://doi.org/10.1074/jbc.M114.566695.
21. Cruz Rodriguez, L., N. N. Foressi, and M. S. Celej. 2023. Modulation of alpha-synuclein phase separation by biomolecules. *Biochim. Biophys. Acta Proteins Proteom.* 1871:140885. https://doi.org/10.1016/j.bbapap.2022.140885.
22. Celej, M. S., E. A. Jares-Erijman, and T. M. Jovin. 2008. Fluorescent N-arylaminonaphthalene sulfonate probes for amyloid aggregation of alpha-synuclein. *Biophys. J.* 94:4867–4879. https://doi.org/10.1529/biophysj.107.125211.
23. Fereidouni, F., A. N. Bader, and H. C. Gerritsen. 2012. Spectral phasor analysis allows rapid and reliable unmixing of fluorescence microscopy spectral images. *Opt. Express.* 20:12729–12741. https://doi.org/10.1364/OE.20.012729.
24. Malacrida, L., D. M. Jameson, and E. Gratton. 2017. A multidimensional phasor approach reveals LAURDAN photophysics in NIH-3T3 cell membranes. *Sci. Rep.* 7:9215. https://doi.org/10.1038/s41598-017-08564-z.

25. Mangiarotti, A., M. Siri, …, R. Dimova. 2023. Biomolecular condensates modulate membrane lipid packing and hydration. *Nat. Commun.* 14:6081. https://doi.org/10.1038/s41467-023-41709-5.

26. Socas, L. B. P., and E. E. Ambroggio. 2022. Introducing the multi-dimensional spectral phasors: a tool for the analysis of fluorescence excitation-emission matrices. *Methods Appl. Fluoresc.* 10:025003. https://doi.org/10.1088/2050-6120/ac5389.

27. Mangiarotti, A., N. Chen, …, R. Dimova. 2023. Wetting and complex remodeling of membranes by biomolecular condensates. *Nat. Commun.* 14:2809. https://doi.org/10.1038/s41467-023-37955-2.

28. Bader, A. N., N. V. Visser, …, A. J. W. G. Visser. 2014. Phasor approaches simplify the analysis of tryptophan fluorescence data in protein denaturation studies. *Methods Appl. Fluoresc.* 2:045001. https://doi.org/10.1088/2050-6120/2/4/045001.

29. Recoulat Angelini, A. A., E. A. Roman, and F. L. González Flecha. 2024. The Structural Stability of Membrane Proteins Revisited: Combined Thermodynamic and Spectral Phasor Analysis of SDS-induced Denaturation of a Thermophilic Cu(I)-transport ATPase. *J. Mol. Biol.* 436:168689. https://doi.org/10.1016/j.jmb.2024.168689.

30. Villar, S. F., J. Dalla-Rizza, …, A. Denicola. 2022. Fluorescence Lifetime Phasor Analysis of the Decamer-Dimer Equilibrium of Human Peroxiredoxin 1. *Int. J. Mol. Sci.* 23:5260. https://doi.org/10.3390/ijms23095260.

31. Fasano, M., S. Curry, …, P. Ascenzi. 2005. The extraordinary ligand binding properties of human serum albumin. *IUBMB Life.* 57:787–796. https://doi.org/10.1080/15216540500404093.

32. He, X. M., and D. C. Carter. 1992. Atomic structure and chemistry of human serum albumin. *Nature.* 358:209–215. https://doi.org/10.1038/358209a0.

33. Eftink, M. R. 1994. The use of fluorescence methods to monitor unfolding transitions in proteins. *Biophys. J.* 66:482–501. https://doi.org/10.1016/s0006-3495(94)80799-4.

34. Ahmad, B., M. Z. Ahmed, …, R. H. Khan. 2005. Guanidine hydrochloride denaturation of human serum albumin originates by local unfolding of some stable loops in domain III. *Biochim. Biophys. Acta.* 1750:93–102. https://doi.org/10.1016/j.bbapap.2005.04.001.

35. Thoke, H. S. 2014. Characterization of Polarity Sensitive Fluorescent Probes in Crowded Environments, Master Thesis. University of Southern Denmark.

36. Galantini, L., C. Leggio, and N. V. Pavel. 2008. Human serum albumin unfolding: a small-angle X-ray scattering and light scattering study. *J. Phys. Chem. B.* 112:15460–15469. https://doi.org/10.1021/jp806821e.

37. Burgos, M. I., S. A. Dassie, and G. D. Fidelio. 2023. The effect of denaturants on protein thermal stability analyzed through a theoretical model considering multiple binding sites. *Biochim. Biophys. Acta, Proteins Proteomics.* 1871:140920. https://doi.org/10.1016/j.bbapap.2023.140920.

38. Handa, A. K., T. Fatima, and A. K. Mattoo. 2018. Polyamines: Bio-Molecules with Diverse Functions in Plant and Human Health and Disease. *Front. Chem.* 6:10. https://doi.org/10.3389/fchem.2018.00010.

39. Antony, T., W. Hoyer, …, V. Subramaniam. 2003. Cellular polyamines promote the aggregation of alpha-synuclein. *J. Biol. Chem.* 278:3235–3240. https://doi.org/10.1074/jbc.M208249200.

40. Wetzel, R. 2006. Kinetics and thermodynamics of amyloid fibril assembly. *Acc. Chem. Res.* 39:671–679. https://doi.org/10.1021/ar050069h.

41. Bertoncini, C. W., Y. S. Jung, …, M. Zweckstetter. 2005. Release of long-range tertiary interactions potentiates aggregation of natively unstructured alpha-synuclein. *Proc. Natl. Acad. Sci. USA.* 102:1430–1435. https://doi.org/10.1073/pnas.0407146102.

42. Maurer, M., and C. Oostenbrink. 2019. Water in protein hydration and ligand recognition. *J. Mol. Recogn.* 32:e2810. https://doi.org/10.1002/jmr.2810.

43. Ball, P. 2008. Water as an active constituent in cell biology. *Chem. Rev.* 108:74–108. https://doi.org/10.1021/cr068037a.

44. Stephens, A. D., and G. S. Kaminski Schierle. 2019. The role of water in amyloid aggregation kinetics. *Curr. Opin. Struct. Biol.* 58:115–123. https://doi.org/10.1016/j.sbi.2019.06.001.

45. Camino, J. D., P. Gracia, and N. Cremades. 2021. The role of water in the primary nucleation of protein amyloid aggregation. *Biophys. Chem.* 269:106520. https://doi.org/10.1016/j.bpc.2020.106520.

46. Pavlova, A., E. R. McCarney, …, S. Han. 2009. Site-specific dynamic nuclear polarization of hydration water as a generally applicable approach to monitor protein aggregation. *Phys. Chem. Chem. Phys.* 11:6833–6839. https://doi.org/10.1039/b906101k.

47. Chakraborty, I., R. K. Kar, …, A. Bhunia. 2021. Solvent Relaxation NMR: A Tool for Real-Time Monitoring Water Dynamics in Protein Aggregation Landscape. *ACS Chem. Neurosci.* 12:2903–2916. https://doi.org/10.1021/acschemneuro.1c00262.

48. Hoyer, W., T. Antony, …, V. Subramaniam. 2002. Dependence of alpha-synuclein aggregate morphology on solution conditions. *J. Mol. Biol.* 322:383–393. https://doi.org/10.1016/s0022-2836(02)00775-1.

49. Fauerbach, J. A., D. A. Yushchenko, …, E. A. Jares-Erijman. 2012. Supramolecular non-amyloid intermediates in the early stages of alpha-synuclein aggregation. *Biophys. J.* 102:1127–1136. https://doi.org/10.1016/j.bpj.2012.01.051.

50. Gracia, P., J. D. Camino, …, N. Cremades. 2020. Multiplicity of alpha-Synuclein Aggregated Species and Their Possible Roles in Disease. *Int. J. Mol. Sci.* 21:8043. https://doi.org/10.3390/ijms21218043.

51. Rai, S. K., A. Savastano, …, M. Zweckstetter. 2021. Liquid-liquid phase separation of tau: From molecular biophysics to physiology and disease. *Protein Sci.* 30:1294–1314. https://doi.org/10.1002/pro.4093.

52. Boyko, S., and W. K. Surewicz. 2022. Tau liquid-liquid phase separation in neurodegenerative diseases. *Trends Cell Biol.* 32:611–623. https://doi.org/10.1016/j.tcb.2022.01.011.

53. Brodin, L., D. Milovanovic, …, O. Shupliakov. 2022. alpha-Synuclein in the Synaptic Vesicle Liquid Phase: Active Player or Passive Bystander? *Front. Mol. Biosci.* 9:891508. https://doi.org/10.3389/fmolb.2022.891508.

54. Mukherjee, S., A. Sakunthala, …, S. K. Maji. 2023. Liquid-liquid Phase Separation of alpha-Synuclein: A New Mechanistic Insight for alpha-Synuclein Aggregation Associated with Parkinson's Disease Pathogenesis. *J. Mol. Biol.* 435:167713. https://doi.org/10.1016/j.jmb.2022.167713.

55. Cruz Rodriguez, L., N. N. Foressi, and M. S. Celej. 2024. Liquid-liquid phase separation of tau and alpha-synuclein: A new pathway of overlapping neuropathologies. *Biochem. Biophys. Res. Commun.* 741:151053. https://doi.org/10.1016/j.bbrc.2024.151053.

56. Siegert, A., M. Rankovic, …, M. Zweckstetter. 2021. Interplay between tau and alpha-synuclein liquid-liquid phase separation. *Protein Sci.* 30:1326–1336. https://doi.org/10.1002/pro.4025.

57. Gracia, P., D. Polanco, …, N. Cremades. 2022. Molecular mechanism for the synchronized electrostatic coacervation and co-aggregation of alpha-synuclein and tau. *Nat. Commun.* 13:4586. https://doi.org/10.1038/s41467-022-32350-9.

58. Foressi, N. N., L. C. Rodríguez, and M. S. Celej. 2023. Heterotypic liquid-liquid phase separation of tau and alpha-synuclein: Implications for overlapping neuropathologies. *Biochim. Biophys. Acta, Proteins Proteomics.* 1871:140950. https://doi.org/10.1016/j.bbapap.2023.140950.

59. Ambadi Thody, S., H. D. Clements, …, M. K. Rosen. 2024. Small-molecule properties define partitioning into biomolecular condensates. *Nat. Chem.* 16:1794–1802. https://doi.org/10.1038/s41557-024-01630-w.

60. Kilgore, H. R., P. G. Mikhael, …, R. A. Young. 2024. Distinct chemical environments in biomolecular condensates. *Nat. Chem. Biol.* 20:291–301. https://doi.org/10.1038/s41589-023-01432-0.

61. Ambroggio, E. E., G. S. Costa Navarro, …, A. V. Gamarnik. 2021. Dengue and Zika virus capsid proteins bind to membranes and self-assemble into liquid droplets with nucleic acids. *J. Biol. Chem.* 297:101059. https://doi.org/10.1016/j.jbc.2021.101059.

62. Alberti, S., and D. Dormann. 2019. Liquid-Liquid Phase Separation in Disease. *Annu. Rev. Genet.* 53:171–194. https://doi.org/10.1146/annurev-genet-112618-043527.

63. Babinchak, W. M., and W. K. Surewicz. 2020. Liquid-Liquid Phase Separation and Its Mechanistic Role in Pathological Protein Aggregation. *J. Mol. Biol.* 432:1910–1925. https://doi.org/10.1016/j.jmb.2020.03.004.

64. Linsenmeier, M., L. Faltova, …, P. Arosio. 2023. The interface of condensates of the hnRNPA1 low-complexity domain promotes formation of amyloid fibrils. *Nat. Chem.* 15:1340–1349. https://doi.org/10.1038/s41557-023-01289-9.

65. Lipiński, W. P., B. S. Visser, …, E. Spruijt. 2022. Biomolecular condensates can both accelerate and suppress aggregation of α-synuclein. *Sci. Adv.* 8:eabq6495. https://doi.org/10.1126/sciadv.abq6495.

66. Emmanouilidis, L., E. Bartalucci, …, F. H. T. Allain. 2024. A solid beta-sheet structure is formed at the surface of FUS droplets during aging. *Nat. Chem. Biol.* 20:1044–1052. https://doi.org/10.1038/s41589-024-01573-w.

67. Pantoja-Uceda, D., C. Stuani, …, M. Mompeán. 2021. Phe-Gly motifs drive fibrillization of TDP-43's prion-like domain condensates. *PLoS Biol.* 19:e3001198. https://doi.org/10.1371/journal.pbio.3001198.

68. Shen, Y., A. Chen, …, T. P. J. Knowles. 2023. The liquid-to-solid transition of FUS is promoted by the condensate surface. *Proc. Natl. Acad. Sci. USA.* 120:e2301366120. https://doi.org/10.1073/pnas.2301366120.

69. Das, T., F. K. Zaidi, …, T. Mittag. 2025. Metastable condensates suppress conversion to amyloid fibrils. Preprint at bioRxiv. https://doi.org/10.1101/2024.02.28.582569.

70. Ray, S., N. Singh, …, S. K. Maji. 2020. alpha-Synuclein aggregation nucleates through liquid-liquid phase separation. *Nat. Chem.* 12:705–716. https://doi.org/10.1038/s41557-020-0465-9.

71. Morris, O. M., Z. Toprakcioglu, …, M. Vendruscolo. 2024. Aggregation of the amyloid-beta peptide (Abeta40) within condensates generated through liquid-liquid phase separation. *Sci. Rep.* 14:22633. https://doi.org/10.1038/s41598-024-72265-7.